ARTICLE

Mechanical Anisotropy and Tabletability of Famotidine Polymorphs

Received 00th January 20xx,
Accepted 00th January 20xx

DOI: 10.1039/x0xx00000x

Pratik P. Upadhyay[a], Manish Kumar Mishra[b], Upadrasta Ramamurty[c,d] and Andrew D. Bond*[a,e]

In the drug development process, early characterization of solid forms can help to envisage the bulk processability of a powder, which should assist in selecting an optimal solid form. In this context, we examine the mechanical properties of two polymorphs of famotidine, form A and form B, using nanoindentation on multiple faces of single crystals to assess the degree of anisotropy. Crystals of form A obtained from acetonitrile typically present two different faces suitable for indentation. For form B, crystallization from ethanol yields two different crystal habits, which together allow for indentation on two crystal faces. On the basis of the two faces examined for each polymorph, form B shows a highly anisotropic elastic modulus (*E*), but an approximately isotropic hardness (*H*), while form A shows approximately isotropic values for both *E* and *H*. Hydrogen-bonding patterns and energy-vector models indicate a 3-D nature for the crystal structure of form A, but an apparent 2-D nature for form B, which is qualitatively consistent with the observed difference in anisotropy. The structure of form B contains regions expected to act as slip planes but the similarity between the *H* values obtained for forms A and B indicates that these do not impart significant plasticity, apparently due to a corrugated topology. For sieved powder samples with particle size less than 125 μm, form A displays better tabletability than form B, especially at higher applied pressures. The overall isotropic nature of the mechanical properties in form A, compared to the highly anisotropic elastic response of form B, appears to be the important indicator of the comparative tabletability of these two polymorphs.

Introduction

Solid-form screening is an essential part of the late drug discovery and early drug development pipelines. The primary aim is often to search for solubility or stability enhancement, with less initial emphasis likely to be given to evaluating materials properties.[1-5] For solid dosage forms, material properties can have a pronounced effect on the manufacturability of the drug product, so it is desirable also to evaluate such properties at an early stage. Technological advancements in techniques such as compaction simulation,[6-9] atomic force microscopy[10] and nanoindentation[11-14] enable assessment of materials properties using quantities of material that are likely to be available during screening. Thus, the continued development of the relationships between structure and relevant materials properties, using information available from such techniques, remains a priority.

In this context, it is valuable to study polymorphs of active pharmaceutical ingredients (APIs), since these provide an opportunity to assess the influence of differing crystal structures for the same molecular API. We focus here on mechanical properties, especially elastic modulus (*E*) and hardness (*H*), assessed by nanoindentation on single crystals. These have been correlated with important pharmaceutical properties like solubility[15], desolvation,[16-17] milling behaviour[18-19] and tabletability.[20-22] One advantage of nanoindentation is that it can be used to probe a crystal from multiple directions, allowing an examination of the interaction anisotropy that generally exists in molecular crystals, and which can be crucial for materials selection in engineering applications.[17,23-26] For example, plastic deformation in a crystalline material is linked to the existence of slip planes, and significantly different mechanical properties are anticipated along directions orientated differently with respect to such slip planes. Hence, correlation between nanoindentation results and bulk behaviour generally requires analysis of multiple indentation directions. The extent to which this can be achieved is often limited by the crystal faces that can be developed during crystallization, so to maximize the value of nanoindentation results for a given material might also require extensive crystallization trials to yield a range of suitable crystal habits.

This paper considers two polymorphs of famotidine (Figure 1).[27] Form B (denoted FB; m.p. ≈ 162 °C) is the commercialized form, which demonstrates a higher dissolution rate than Form A (denoted FA; m.p. ≈ 169 °C). FB is a metastable polymorph, reported to convert to thermodynamically stable FA during

[a] *Department of Pharmacy, University of Copenhagen, Universitetsparken 2, 2100 Copenhagen, Denmark.*
[b] *Department of Chemistry (SAS), Vellore Institute of Technology (VIT), Vellore 632014, Tamil Nadu, India.*
[c] *School of Mechanical and Aerospace Engineering, Nanyang Technological University, Singapore 639798, Singapore.*
[d] *Institute of Materials Research and Engineering, Agency for Science, Technology and Research (A ⁎STAR), Singapore 138634, Singapore.*
[e] *Yusuf Hamied Department of Chemistry, University of Cambridge, Lensfield Road, Cambridge, CB2 1EW, UK. Email: adb29@cam.ac.uk*
Electronic Supplementary Information (ESI) available: experimental and simulated PXRD patterns, face indexing images, SEM images, details of *PIXEL* calculations, energy frameworks from *CrystalExplorer*. See DOI: 10.1039/x0xx00000x

intensive milling[28] or when compressed at higher pressure (> 200 MPa) with higher dwell time.[29] Similar behaviour has been described for the polymorphs of aspirin, for example, where the conversion of form II to form I has been linked to shear instability of form II, as observed by nanoindentation.[30] Nanoindentation responses on famotidine polymorphs have been reported by Egart *et al.* as part of a broader study that correlated average values of single-crystal elasticity with tablet elastic relaxation.[22] For FB, the available faces developed during crystallization limited that study to only one indentation direction, perpendicular to proposed slip planes in the structure. In this work, we have obtained FB crystals with different habits, which enables us to examine the important anisotropy of the indentation response. We find that the elastic response of FB is considerably more anisotropic than that of FA, but that the hardness is comparable and nearly isotropic in both polymorphs. The latter observation is surprising, given that the crystal structure of FB shows a 2-D pattern of hydrogen-bond interactions and contains regions that should be expected to facilitate slip, and hence plastic deformation, more easily. Tabletability studies on sieved bulk powders show that FA displays better tabletability than FB for particle sizes less than 125 μm, especially at higher applied pressures. Hence, the overall isotropic nature of the mechanical properties of FA, compared to the highly anisotropic elastic response of FB, may be the important indicator of the comparative tabletability of these two polymorphs.

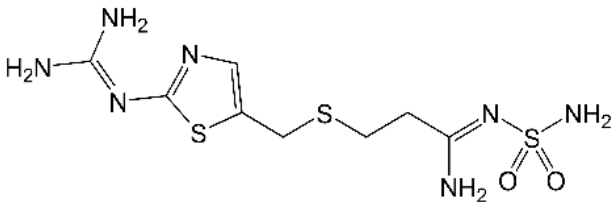

Figure 1. Molecular structure of famotidine.

Experimental

Famotidine was purchased from Jai Radhe Sales, India. The supplied bulk sample was found to be FB, as confirmed by powder X-ray diffraction (PXRD). For crystallisation, HPLC grade methanol, dimethylformamide (DMF) and acetonitrile were purchased from Sigma-Aldrich, and MilliQ water was used. Single crystals of FA and FB were crystallised from acetonitrile and ethanol, respectively, by slow evaporation of a famotidine solution at room temperature. The bulk sample of FA was obtained by adding water to a supersaturated solution of famotidine in DMF with stirring. Bulk FB was obtained by cooling a hot supersaturated solution of famotidine in ethanol. The obtained bulk powders were filtered through 0.45 μm nylon filters and dried overnight in an oven at 50 °C. Polymorphic purity was confirmed by comparing PXRD patterns with reference patterns determined from the crystal structures in the Cambridge Structural Database (CSD).[31] The dried powders were gently crushed without inducing any phase transformation using a mortar and pestle to reduce the particle size, and three different sieve fractions were collected for each polymorph: sieve fraction SF-I, passed through #250 μm and retained on #125 μm; sieve fraction SF-II, passed through #125 μm and retained on #75 μm; sieve fraction SF-III, passed through #75 μm and retained on #36 μm. More specific details of the particle size distribution within each fraction were not established.

X-ray Diffraction

Powder X-ray Diffraction (PXRD) data were collected on a Panalytical X'Pert Pro instrument (Panalytical, Almelo, The Netherlands), equipped with a PIXcel detector using non-monochromated CuKα radiation (λ = 1.5418 Å). The sample was placed in a zero-background Si holder and measured in reflection geometry with sample spinning. Single-crystal X-ray diffraction data were collected on a Bruker D8-QUEST instrument, equipped with a PHOTON-100 detector and an Incoatec IμS microsource (CuKα radiation; λ = 1.5418 Å). Data collection and face indexing were carried out using *APEX3* software (Bruker AXS, Madison, USA).

Nanoindentation

Nanoindentation was performed on single crystals of FA and FB using a nanoindenter (Hysitron Triboindenter, Minneapolis, USA) equipped with in-situ AFM imaging capability. Good quality single crystals of FA and FB, identified using a polarizing microscope, were fixed on the surface of the cleaned metal discs using a thin layer of epoxy resin. A three-sided pyramidal Berkovich diamond indenter (Poisson's ratio = 0.07, tip radius ≈ 100 nm) was used. A maximum force of 5 mN was applied with a loading indentation speed of 0.5 mN s^{-1}. At the maximum peak load of 5 mN, the tip was held for 30 s, before unloading at a rate of 0.5 mN s^{-1}. At least 15 indentations were performed on each crystal face to obtain consistent and reliable average data. The elastic modulus (*E*) and indentation hardness (*H*) were estimated using the Oliver-Pharr method.[32,33] Where significant pile-up was observed during indentation, the *H* value was determined from the maximum load (5 mN) divided by the contact area, *A*, estimated from the AFM images of the indentation impressions.

Computational Methods

The published crystal structures of FA and FB[27] were energy-minimized using dispersion-corrected density functional theory (DFT-D) calculations. Prior to minimization, the positions of all H atoms were normalized using the default settings in *Mercury*.[34] The calculations were made using *CASTEP*[35] via the interface in *Materials Studio* (Accelrys, San Diego, USA). The PBE exchange-correlation functional[36] was applied, with a dispersion correction according to Grimme.[37] The plane-wave basis-set cut-off was set to 340 eV and all other parameters were set to the "Fine" defaults in *Materials Studio*. Unit-cell parameters were constrained to the reported values and the space-group symmetry was imposed. Neither structure produced any significant deviation on minimization, consistent with high-quality crystal structures. Pairwise intermolecular

interaction energies were then calculated using *PIXEL*.[38] The calculations were applied to the DFT-D minimized structures, retaining the H atom positions from those structures. The *PIXEL* output (listed in the Supporting Information) was converted to energy-vector diagrams using *processPIXEL*,[39] and subsequent visualization was carried out using *Mercury*.[34]

Tableting

Tablets of approximately 100 mg were prepared by compressing collected sieve fractions (SF-I, SF-II or SF-III) of the pure famotidine powders using a Gamlen single-punch laboratory tablet press (Gamlen, Nottingham, UK) equipped with calibrated flat-faced punches with a punch speed of 60 mm min^{-1} and a load cell of 500 kg. The punch and die cavity were pre-lubricated using a suspension of 5% w/v magnesium stearate in acetone. The crushing strength of tablets was measured using the same machine with a load cell of 50 kg and 60 mm min^{-1} punch speed. The strength (σ_c in units of MPa) of the tablets was calculated from the force required for crushing, *F* (units of N):

$$\sigma_c = (2F) / (\pi \cdot d \cdot t)$$

where *d* is the diameter of the tablet (mm), and *t* is the thickness (mm). Post-tableting, the tablet was examined using PXRD to confirm that there was no stress-induced phase transformation.

Results and discussion

Crystal Structures

Crystallographic information for FA and FB is listed in Table 1. The structure of FB is included in the CSD in two alternative settings of the same space group. We use the $P2_1/n$ setting in this paper (Table 1), which is consistent with the description used by Egart *et al.* in their nanoindentation study.[22] The alternative $P2_1/c$ setting has unit-cell parameters: $a \approx 17.76$, $b \approx 5.33$, $c \approx 18.31$ Å, $\beta \approx 123.6°$. The structures in $P2_1/n$ and $P2_1/c$ are identical, just described with a different choice of unit cell. Famotidine is a flexible molecule, and FA and FB are conformational polymorphs. In FA, the molecule adopts an open conformation, while FB adopts a folded shape with an internal N–H···N hydrogen bond (Figure 2). In both polymorphs, an intramolecular N–H···N interaction between the guanidine group and the N atom of the thiazole ring imparts planarity to this part of the molecule.

In FA, molecules are linked into centrosymmetric pairs by N–H···N hydrogen bonds (graph set $R_2^2(8)$) between the guanidine groups. The dimers are further connected by N–H···O hydrogen bonds to the O atoms of the sulfonyl groups, defining 2-D sections in the (100) planes (Figure 3a). Further centrosymmetric $R_2^2(8)$ pairs of N–H···N hydrogen bonds are formed at the sulfonyl end of each molecule, linking the aforementioned 2-D sections into an extended 3-D hydrogen-bonded network. In FB, the folded molecules form a complex arrangement of N–H···N and N–H···O hydrogen bonds that define 2-D sections parallel to the $(10\bar{1})$ planes (Figure 3b). The surfaces of these layers comprise principally the hydrophobic CH_2 and CH groups of the famotidine molecule, and the principal

Table 1. Crystallographic information for the famotidine polymorphs.

	Space group	Unit-cell parameters (Å, °)	CSD Refcodes	Melting point (°C)[29]
FA	$P2_1/c$	a = 11.98, b = 7.20, c = 16.81 α = 90, β = 99.8, γ = 90	FOGVIG01[40] FOGVIG04[41] FOGVIG07[27,‡]	169.4
FB[†]	$P2_1/n$	a = 17.05, b = 5.33, c = 17.76 α = 90, β = 116.6, γ = 90	FOGVIG[42] FOGVIG02[43] FOGVIG03[44] FOGVIG05[41] FOGVIG06[27,‡]	161.8

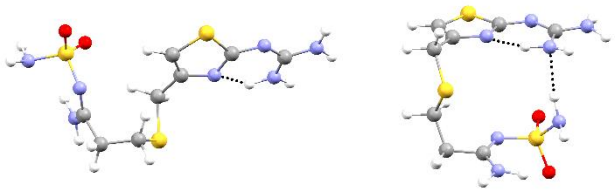

(a) (b)

Figure 2. Molecular conformations in FA (a) and FB (b). The dotted lines indicate intramolecular N–H···N hydrogen bonds.

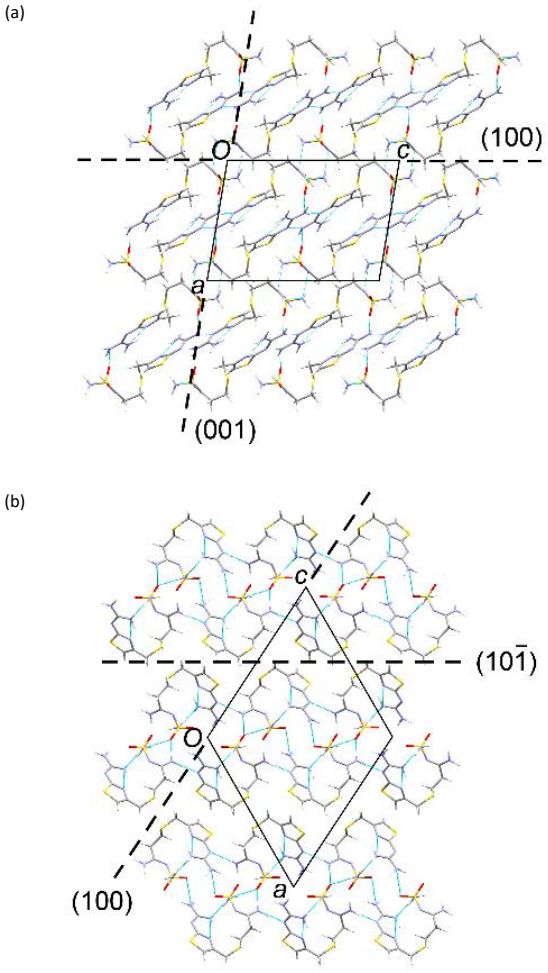

Figure 3. Hydrogen-bond networks in (a) FA and (b) FB. The network in FA is 3-D, while the network in FB is 2-D. Nanoindentation was performed along the directions perpendicular to the indicated crystallographic planes.

contacts between layers are C–H···π and C–H···S. There are no conventional hydrogen bonds between layers. The formation of the 3-D hydrogen-bond network in FA but a 2-D network in FB reflects the additional intramolecular N–H···N hydrogen bond formed in FB (Figure 2). In FB, the presence of the 2-D hydrogen-bonded layers with no specific interactions between them identify $(10\bar{1})$ as probable slip planes (Figure 3b). The same conclusion was reached by Egart *et al.*[22]

Energy-Vector Models

Energy-vector models, developed by Shishkin and co-workers,[45] are a helpful tool to visualize intermolecular interaction energies in crystals. For example, we have used such models to discuss the properties of piroxicam[46] and piracetam.[47] The models comprise lines linking the centroids of molecules, scaled in length according to the magnitude of the interaction energy between the linked molecules. The most stabilizing interaction in the structure is displayed as a complete line, and less stabilizing interactions are scaled proportionally to produce gaps in the lines. Larger gaps indicate interactions that are less stabilizing, and it is intuitive to see the directions in which molecules are most strongly and least strongly bound. The energies refer to the total interaction between molecules, rather than any specific interactions such as hydrogen bonds. Similar methodology is implemented in the program *CrystalExplorer*,[48] which yields closely comparable results for FA and FB (see ESI).

Energy-vector models for FA and FB, based on *PIXEL* calculations, are shown in Figure 4. As would be anticipated from the 3-D hydrogen-bond network, the model for FA appears to be principally 3-D. By contrast, the model for FB shows a clear 2-D structure, with significant gaps between the sections parallel to the $(10\bar{1})$ planes. This confirms the energetic basis for assignment of $(10\bar{1})$ as probable slip planes.

Nanoindentation

Good quality single crystals of FA, obtained from acetonitrile solution, revealed two major faces suitable for indentation: {001} and {100}. These are the same faces studied by Egart *et al.*[22] Crystals of FB, obtained from ethanol solution, showed either a lathlike habit with major face $\{10\bar{1}\}$ or a columnar habit with the {100} face accessible for indentation (see ESI). Egart *et al.* studied the $\{10\bar{1}\}$ face of FB, but not the {100} face. We performed indentation on both FA and FB in the directions perpendicular to the four identified crystal faces. Representative indentation force (*P*) versus depth of penetration (*h*) responses are displayed in Figure 5, and values of *E* and *H* derived from them are listed in Table 2.

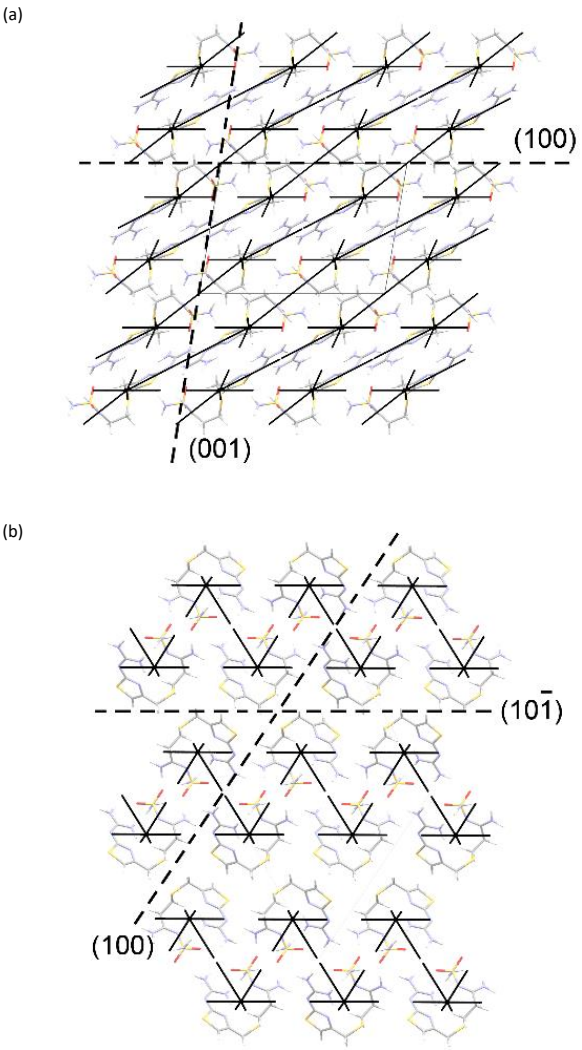

Figure 4. Energy-vector models for (a) FA and (b) FB, based on *PIXEL* calculations. The orientation of the diagrams is identical to that in Figure 3.

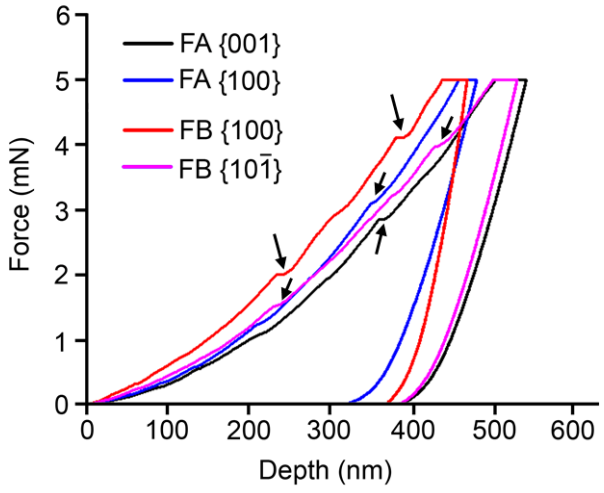

Figure 5. Representative load-displacement (P-h) responses for indentation on single crystals of FA and FB.

Table 2. Elastic modulus and hardness values for FA and FB.

	H-bond dimension	Face	d_{hkl} (Å)	Average $h_{pop\text{-}in}$ (nm)	Present study			Egart *et al.*[22]		
					Elastic modulus (*E*) (GPa)	Hardness (*H*) (MPa)	E:H ratio	Elastic modulus (*E*) (GPa)	Hardness (*H*) (MPa)	E:H ratio
FA	3-D	{100}	11.80	3 and 6	19.16 ± 0.18	831 ± 19	23.1	22.6 ± 2.0	1580 ± 400	14.3
		{001}	16.56	4, 8, and 12	17.20 ± 0.42	703 ± 4	24.5	20.1 ± 1.2	1330 ± 160	15.1
FB	2-D	{100}	15.25	5, 10, 15, and 20	29.18 ± 0.74	710 ± 30	41.1	not studied		—
		{10$\bar{1}$}	14.79	4, 7, and 14	17.79 ± 0.22	643 ± 23	27.7	19.5 ± 0.4	840 ± 160	23.2

Figure 5 shows that the residual depths of penetration after complete unloading on the {100} faces of both FA and FB are lower than those recorded on the other faces of the respective crystals. The loading segments of all the *P*–*h* responses are serrated in nature; in particular, the {100} face of FB showed distinct and large serrations. Prior nanoindentation studies on molecular crystals have established that such serrations (often referred to as "pop-ins") are a result of discontinuous plastic deformation through sudden slip of molecular layers, with the average values of the displacement burst magnitudes, $h_{pop\text{-}in}$, typically scaling with integer multiples of the interplanar *d* spacing, d_{hkl} of their corresponding faces.[12] Data given in Table 2 show a reasonable correlation between $h_{pop\text{-}in}$ and d_{hkl}. The topographic images of the indents (obtained using the same indenter tip, but in the scanning mode) are displayed in Figure 6. These show material pile-up along the edges of the indenter impressions on both the {100} faces of FA and FB, whereas no significant pile up is observed on the FA {001} or FB {10$\bar{1}$} faces.

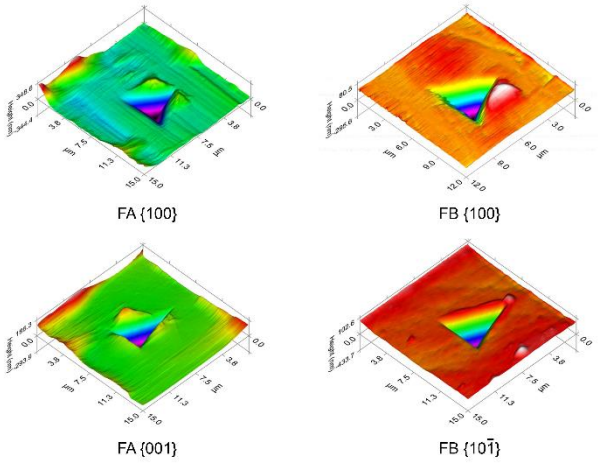

Figure 6. AFM images of nanoindentation indents of FA (left) and FB (right).

Table 2 shows that, on average, FB is softer while being stiffer, especially the *E* value obtained on its {100} face being nearly 50% higher than the next highest value. The anisotropy in *H* is not significant in either FA or FB, and the elastic anisotropy in FA is also marginal. For FA, the ratios of *E* and *H* on the two measured faces, {100}:{001} = 1.11 (*E*) and 1.19 (*H*), suggest it to be nearly isotropic from the perspective of its mechanical properties. Similar ratios for *E* (1.12) and *H* (1.19) were found by Egart *et al.* for the same indented faces of FA,[22] although the actual *E* and *H* values are different from our data. Such differences in nanoindentation results reported by different sets of investigators have been noted for a number of other APIs, including aspirin,[30,49] saccharin[20,23] and caffeine-glutaric acid.[50,51] They arise due to the different experimental parameters employed, such as the mode of loading (continuous stiffness measurement *vs.* quasi-static indentation), rate of loading, indenter geometry, maximum depth of penetration, quality of the crystal (especially the surface) and how well it is mounted, *etc.* For FB, the ratios of mechanical properties for {100}:{10$\bar{1}$} = 1.64 (*E*) and 1.11 (*H*) demonstrate that it exhibits high elastic anisotropy, which is significantly larger than other polymorphic APIs for which data are available, *e.g.* piracetam FII (1.07),[50] aspirin FI (1.60),[30] and felodipine FII (in the range 1.0–1.5 for two different observed structural domains).[52] The high anisotropy for FB is caused by the particularly high *E* value (29.18 ± 0.74 GPa) measured for the {100} face.

Structure-property correlation

The principal feature to emerge from the new nanoindentation results is the significantly anisotropic nature of FB, in terms of *E*, accompanied by a much more isotropic *H*. For FA, both *E* and *H* are approximately isotropic. For molecular crystals, *E* is sensitive to the nature and number of the intermolecular interactions,[53] while *H* broadly reflects the resistance of a material to plastic deformation, typically determined by the presence or absence of facile slip planes oriented favourably with respect to the indentation direction (*i.e.* the resolved shear stress on them from geometric considerations is maximum).[54] For FA, the energy-vector diagram (Figure 4a) shows continuous lines running along the diagonal of the *ac* face of the unit cell (crystallographic direction [$\bar{1}$01]). These represent rows of molecules forming two different, but approximately isoenergetic, pairwise intermolecular interactions involving the previously described $R_2^2(8)$ hydrogen-bond motifs. The interactions between these rows of molecules produce a triangular mesh in the energy-vector diagram and the two indentation directions are approximately aligned with the sides of these triangles (Figure 7a). The apparent regularity of the mesh is qualitatively consistent with the comparable *E* values along the two measured indentation directions. For plastic deformation, which is reflected in *H*, the slip plane is oriented at an approximately similar angle for both indentation directions. This is probably the reason for the similar *H* values measured for FA.

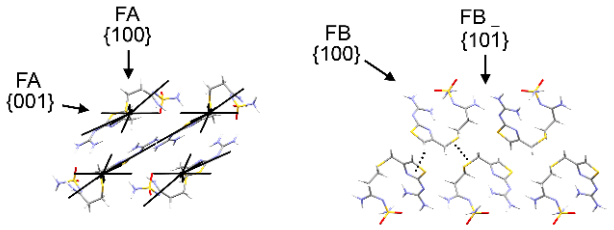

Figure 7. (a) Relationship between the indentation directions and energy-vector diagram in FA. (b) Relationship between the indentation directions and corrugated region between the 2-D sections parallel to of (10$\bar{1}$) in FB. The dotted lines highlight edge-to-face interactions between thiazole rings and side-on interactions between thioether units.

For FB, the energy-vector diagram suggests that the structure contains "strong" layers parallel to the (10$\bar{1}$) planes, and that the elastic response is likely to be governed by the regions between these layers. The interlayer regions show a corrugated nature involving edge-to-face (C–H···π) interactions between thiazole rings and side-on interactions between the thioether (–CH_2SCH_2–) units of famotidine (Figure 7b). Indentation on {100} should allow the C—H···π interaction to distort laterally, with minimal compression of the H···ring distance, but compress the spacing between the thioether units perpendicular to their length. Indentation on {10$\bar{1}$} of FB should cause a mixture of compression and lateral movement for both interaction types. We assume that the highly anisotropic elastic response is related to this difference. The corrugated nature of the inter-layer region is also likely to be the reason for the failure of (10$\bar{1}$) in FB to act as slip planes, leading to the comparable hardness values for FA and FB along the directions that have been examined.

Bulk powder tabletability

Tabletability of the bulk powder, obtained by plotting the tensile strength of tablets prepared with increasing pressure, is one of the most important quality parameters associated with the friability[55] and dissolution time[56,57] of tablets. The ability of crystals to undergo plastic deformation is considered to be one of the primary contributors to tablet strength.[58–60] This is because plastic deformation allows the crystals to change shape permanently in response to an applied load during compression and enhance the bond between various neighbouring grains. Tabletability studies were made for the bulk powders of FA and FB. To account for contributions from particle size, large single crystals were gently crushed using a mortar and pestle and three sieve fractions were studied, as outlined in the Experimental Section. The results (Figure 8) show effectively identical behaviour for FA and FB for the largest sieve fraction (SF-I, retained on #125 μm). The two further sieve fractions (SF-II, retained on #75 μm, and SF-III, retained on #36 μm) formed considerably stronger tablets, with SF-III exhibiting marginally better strength than SF-II. In both cases, FA shows better tabletability than FB, especially at higher applied pressures, although the uncertainty in the measured strength also appears to increase with pressure.

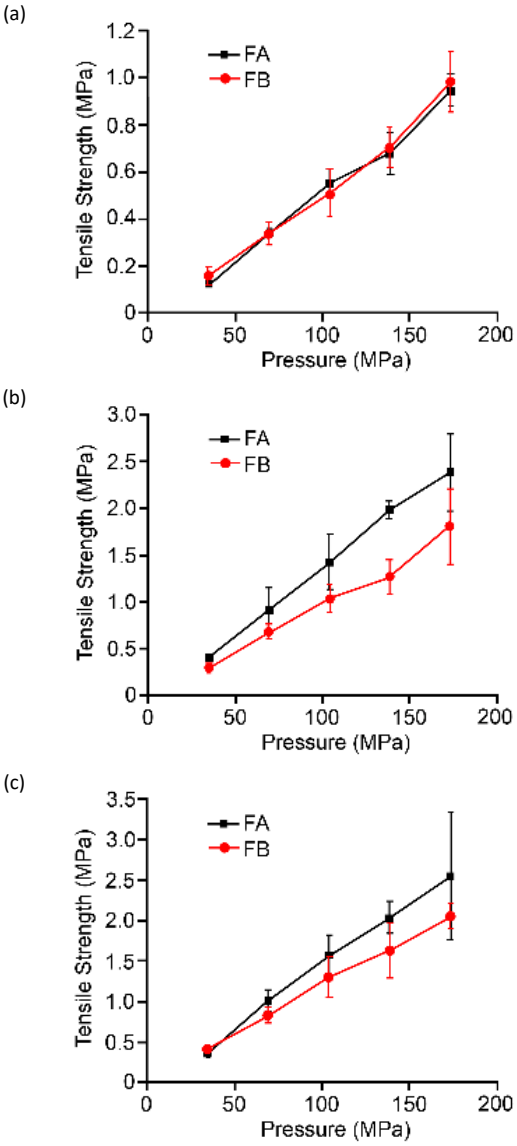

Figure 8. Tabletability of FA and FB using three different sieve fractions (a) SF-I (retained on #125 μm), (b) SF-II (retained on #75 μm), (c) SF-III (retained on #36 μm).

The mechanical stability of a pharmaceutical tablet largely depends on the contributions of both bonding strength and bonding area among the powder particles in the tablet. The bonding area alters with particle size or shape and compaction pressure, while the bonding strength depends on molecular packing and intermolecular interactions.[59] For SF-I, the results are dominated by the size/shape of the particles rather than the underlying crystal structures. The lower strength compared to the other sieve fractions is consistent with the expected tendency for the larger particles to form more porous tablets. For SF-II and SF-III, the comparatively better tableting behaviour of FA over FB is possibly due to (a) the overall mechanical isotropy in FA, although it is marginally harder than FB, and (b) the large E value of FB in the {100} orientation. When powders are compressed, randomly oriented single crystals (which constitute the powder particles) that are next to each other

have to plastically 'flow' together so as to form a high bonding strength among the adjacent particles in the tablet.[59] The more structurally and mechanically isotropic the stiff particles are, the more likely they can accommodate such flow congruently. A stiff crystal, even in only one direction as in FB, would require the application of much larger compressive loads for obtaining the same levels of deformation strains. It can be noted that if the particle size is already sufficiently small, the increase in bonding area through plastic deformation is somewhat diminished. Hence, the enhancement in the bonding strength becomes more important for achieving high tensile strength or tabletability during compaction.[59]

With regard to the elasticity, Egart *et al.* applied average *E* values to correlate with elastic relaxation of tablets prepared from pure powders of the studied APIs, where the value for FB was based on the value for $\{10\bar{1}\}$ alone.[22] The significantly larger *E* found here for {100} means that the true average for FB must be larger. Although this affects the details of the established relationship, it does not alter the overall conclusion that there is a positive correlation between tablet elastic relaxation and the average *E* of the underlying crystal structure for the set of APIs that was studied.[22]

Conclusions

The possibility to study different crystal faces of FB, by realizing different crystal habits during crystallization trials, adds significant value to the nanoindentation study of the famotidine polymorphs. Reasonable analysis of the crystal structures of FA and FB on the basis of hydrogen bonding and intermolecular interaction energies suggests that FB is likely to show a greater degree of anisotropy than FA, and particularly greater plasticity on account of apparent slip planes. Our studies show that the elastic response of FB is indeed more anisotropic than FA, but that the hardness of the polymorphs is comparable, and approximately isotropic, on the basis of the two crystal faces that have been examined. For smaller particle sizes, where the influence of tablet porosity is diminished, FA shows better tabletability than FB, especially at higher applied pressures. Hence, the isotropic nature of the mechanical properties in FA, compared to the highly anisotropic elastic response of FB, may be the important indicator of the comparative tabletability of these two polymorphs.

Author Contributions

The experimental aspects of this investigation were carried out by PPU and MKM, under the supervision of ADB and UR, respectively. All authors contributed to data analysis and interpretation, and to writing of the manuscript.

Conflicts of interest

There are no conflicts to declare.

Acknowledgements

We thank the Danish Council for Independent Research | Natural Sciences (DFF-1323-00122) and Department of Pharmacy, University of Copenhagen for funding this work.

Notes and references

† In the CSD, FOGVIG02, FOGVIG03 and FOGVIG06 are described in space group $P2_1/c$, while FOGVIG and FOGIVG05 are described in $P2_1/n$. These structures are identical, just described with a different choice of unit cell.

‡ The FA/FB designation for FOGVIG06 and FOGVIG07 is incorrect in the CSD. This follows uncertainty introduced in the paper by Ferenczy *et al*. In that paper, the labels for the two forms are exchanged in the tables listing crystallographic and geometrical information (Tables 1–5 in Ref. 27), while the figures correctly show FA with the open conformation and FB with the closed conformation. It is not clear whether the computational conclusions are derived from the crystallographic models labelled as in the tables or as in the figures.

1 C. R. Gardner, C. T. Walsh and O. Almarsson, *Nat. Rev. Drug Discov.* 2004, **3**, 926.
2 J. M. Miller, B. M. Collman, L. R. Greene, D. J. W. Grant and A. C. Blackburn, *Pharm. Dev. Technol.* 2005, **10**, 291.
3 S. S. Bharate and R. A. Vishwakarma, *Expert Opin. Drug Del.* 2013, **10**, 1239.
4 M. D. Ticehurst and I. Marziano, *J. Pharm. Pharmacol.* 2015, **67**, 782.
5 J. Aaltonen, M. Allesø, S. Mirza, V. Koradia, K. C. Gordon and J. Rantanen, *Eur. J. Pharm. Biopharm.* 2009, **71**, 23.
6 M. Asgharnejad and D. E. Storey, *Drug Dev. Ind. Pharm.* 1996, **22**, 967.
7 J. M. Katz, R. Roopwani and I. S. Buckner, *J. Pharm. Sci.* 2013, **102**, 3687.
8 C. C. Sun, *Int. J. Pharmaceut.* 2006, **32**, 94.
9 M. Çelik and K. Marshall, *Drug Dev. Ind. Pharm.* 1989, **15**, 759.
10 E. H. H. Chow, D.-K. Bučar and W. Jones, *Chem. Commun.* 2012, **48**, 9210.
11 U. Ramamurty and J.-I. Jang, *CrystEngComm,* 2014, **16**, 12.
12 S. Varughese, M. S. R. N. Kiran, U. Ramamurty and G. R. Desiraju, *Angew. Chem. Int. Ed.* 2013, **52**, 2701.
13 M. K. Mishra, U. Ramamurty and G. R. Desiraju, *Curr. Opin. Solid State Mater. Sci.* 2016, **20**, 361.
14 B. P. A. Gabriele, C. J. Williams, M. E. Lauer, B. Derby and A. J. Cruz-Cabeza, *Cryst. Growth Des.* 2020, **20**, 5956.
15 M. K. Mishra, P. Sanphui, U. Ramamurty and G. R. Desiraju, *Cryst. Growth Des.* 2014, **14**, 3054.
16 M. S. R. N. Kiran, S. Varughese, U. Ramamurty and G. R. Desiraju, *CrystEngComm*, 2012, **14**, 2489.
17 S. SeethaLekshmi, M. S. R. N. Kiran, U. Ramamurty and S. Varughese, *Cryst. Growth Des*. 2020, **20**, 442.
18 M. Meier, E. John, D. Wieckhusen, W. Wirth and W. Peukert, *Powder Technol.* 2009, **188**, 301.
19 L. J. Taylor, D. G. Papadopoulos, P. J. Dunn, A. C. Bentham, N. J. Dawson, J. C. Mitchell and M. J. Snowden, *Org. Proc. Res. Dev.* 2004, **8**, 674.
20 S. Chattoraj, L. Shi, M. Chen, A. Alhalaweh, S. Velaga and C. C. Sun, *Cryst. Growth Des.* 2014, **14**, 3864.
21 M. Egart, I. Ilić, B. Janković, N. Lah and S. Srčič, *Int. J. Pharm.* 2014, **472**, 347.
22 M. Egart, B. Janković, N. Lah, I. Ilić and S. Srčič, *Pharm. Res.* 2015, **32**, 469.
23 M. S. R. N. Kiran, S. Varughese, C. M. Reddy, U. Ramamurty and G. R. Desiraju, *Cryst. Growth Des*. 2010, **10**, 4650.

24 E. Hadjittofis, M. A. Isbell, V. Karde, S. Varghese, C. Ghoroi, and J. Y. Y. Heng, *Pharm. Res.* 2018, **35**, 100.
25 A. Jain, H. S. Shah, P. R. Johnson, A. S. Narang, K. R. Morris and R. V. Haware, *Eur. J. Pharm. Biopharm.* 2018, **132**, 83.
26 R. M. Mohamed, M. K. Mishra, L. M. Al-Harbi, M. S. Al-Ghamdi and U. Ramamurty, *RSC Adv.* 2015, **5**, 64156.
27 G. G. Ferenczy, L. Párkányi, J. G. Ángyán, A. Kálmán and B. Hegedűs, *J. Mol. Struct.: THEOCHEM*, 2000, **503**, 73.
28 W.-T. Cheng, S.-Y. Lin and M.-J. Li, *J. Raman Spectrosc.* 2007, **38**, 1595.
29 M. V. Roux, J. Z. Dávalos and P. Jiménez, *Thermochim. Acta*, 2002, **394,** 19.
30 S. Varughese, M. S. R. N. Kiran, K. A. Solanko, A. D. Bond, U. Ramamurty and G. R. Desiraju, *Chem. Sci.* 2011, **2**, 2236.
31 C. R. Groom, I. J. Bruno, M. P. Lightfoot and S. C. Ward, *Acta Crystallogr. Sect. B: Struct. Sci., Cryst. Eng. Mater.* 2016, **72**, 171.
32 W. C. Oliver and G. M. Pharr, *J. Mater. Res.* 1992, **7**, 1564.
33 W. C. Oliver and G. M. Pharr, *J. Mater. Res.* 2004, **19**, 3.
34 C. F. Macrae, I. Sovago, S. J. Cottrell, P. T. Galek, P. McCabe, E. Pidcock, M. Platings, G. P. Shields, J. S. Stevens, M. Towler and P. A. Wood, *J. Appl. Crystallogr.* 2020, **53**, 226.
35 S. J. Clark, M. D. Segall, C. J. Pickard, P. J. Hasnip, M. J. Probert, K. Refson and M. C. Payne, *Z. Kristallogr*. 2005, **220**, 567.
36 J. P. Perdew, K. Burke, and M. Ernzerhof, *Phys. Rev. Lett.* 1996, **77**, 3865.
37 S. Grimme, *Comput. Chem.* 2006, **27**, 1787.
38 A. Gavezzotti, *New J. Chem.* 2011, **35**, 1360.
39 A. D. Bond, *J. Appl. Crystallogr.* 2014, **47**, 1777.
40 L. Golič, K. Dijnovič and M. Florjanič, *Acta Crystallogr. Sect. C: Struct. Chem.* 1989, **45**, 1381.
41 J. Overgaard and D. E. Hibbs, *Acta Crystallogr. Sect. A: Found. Adv.* 2004, **60**, 480-487.
42 I. Yanagisawa, Y. Hirata and Y. Ishii, *J. Med. Chem.* 1987, **30**, 1787.
43 K. Shankland, L. McBride, W. I. F. David, N. Shankland and G. Steele, *J. Appl. Crystallogr.* 2002, **35**, 443.
44 A. J. Florence, B. Baumgartner, C. Weston, N. Shankland, A. R. Kennedy, K. Shankland and W. I. F. David, *J. Pharm. Sci.* 2003, **92**, 1930.
45 O. V. Shiskin, V. V. Dyakonenko and A. V. Maleev, *CrystEngComm*, 2012, **14**, 1795.
46 P. P. Upadhyay and A. D. Bond, *CrystEngComm*, 2015, **17**, 5266.
47 P. P. Upadhyay, M. K. Mishra, U. Ramamurty and A. D. Bond, *CrystEngComm*, 2020, **20**, 1226.
48 M. J. Turner, S. P. Thomas, M. W. Shi, D. Jayatilaka and M. A. Spackman, *Chem. Commun*. 2015, **51**, 3735.
49 D. Olusanmi, K. J. Roberts, M. Ghadiri and Y. Ding, *Int. J. Pharm.* 2011, **411**, 49.
50 M. K. Mishra, K. Mishra, A. Narayan, C. M. Reddy and V. R. Vangala, *Cryst. Growth Des.* 2020, **20**, 6306.
51 R. Thakuria, M. D. Eddleston, E. H. H. Chow, L. J. Taylor, B. J. Aldous, J. F. Krzyzaniak and W. Jones, *CrystEngComm*, 2016, **18**, 5296.
52 M. K. Mishra, G. R. Desiraju, U. Ramamurty and A. D. Bond, *Angew. Chem. Int. Ed.* 2014, **126**, 13318.
53 S. Saha, M. K. Mishra, C. M. Reddy and G. R. Desiraju, *Acc. Chem. Res.* 2018, **51**, 2957.
54 M. K. Mishra, U. Ramamurty and G. R. Desiraju, *J. Am. Chem. Soc*. 2015, **137**, 1794.
55 X. Gong, S.-Y. Chang, F. Osei-Yeboah, S. Paul, S. R. Perumalla, L. Shi, W.-J. Sun, Q. Zhou and C. C. Sun, *Int. J. Pharm.* 2015, **493**, 208.
56 S. Kitazawa, I. Johno, Y. Ito, S. Teramura and J. Okada, *J. Pharm. Pharmac.* 1975, **27**, 765.
57 J. T. Jacob and E. M. Plein, *J. Pharm. Sci.* 1968, **57**, 802.
58 S. Datta and D. J. W. Grant, *Nat. Rev. Drug Discov.* 2004, **3**, 42.
59 C. C. Sun, *J Adhes Sci Technol.* 2011, **25**, 483.
60 P. P. Bag, M. Chen, C. C. Sun and C. M. Reddy, *CrystEngComm*, 2012, **14**, 3865.

